Visual Abstract

Influence of hBN and MoS_2 fillers on toughness and thermal stability of carbon fabric-epoxy composites

Yermal Shriraj Rao, B. Shivamurthy, Nanjangud Subbarao Mohan, Nagaraja Shetty*
Department of Mechanical and Industrial Engineering, Manipal Institute of Technology, Manipal Academy of Higher Education, Manipal, Karnataka, India
shrirajrao@gmail.com, http://orcid.org/0000-0003-3653-6977
shiva.b@manipal.edu, http://orcid.org/0000-0002-4273-4884
ns.mohan@manipal.edu, http://orcid.org/0000-0002-1993-3148
nagaraj.shetty@manipal.edu, http://orcid.org/0000-0001-9208-6355

Abstract. Hexagonal boron nitride (hBN) and molybdenum disulfide (MoS_2) fillers of 2 to 8 wt.% influence on toughness, microhardness and thermal stability of carbon fabric-reinforced epoxy composite (CFREC) reported. Mode-I, mixed-mode I/II toughness and microhardness of CFREC improved due to the addition of hBN and MoS_2 separately upto 6 wt.% filler loading. The epoxy matrix in CFREC modified by hBN and MoS_2 strengthens the matrix, deflects the crack path and resists delamination. Toughness reduced beyond 6 wt.% filler addition due to agglomeration and poor fiber-filler-matrix bonding as revealed by the surface morphology of the fracture specimen. Thermal analysis reveals decomposition temperature at 25% weight loss increased from 395 to 430 °C and 395 to 411 °C due to 4 wt.% MoS_2 and 4 wt.% hBN addition to CFREC respectively. Impermeable characteristics of MoS_2 and hBN fillers caused tortuous diffusion path for gas molecules and delayed thermal decomposition.

Keywords. Molybdenum disulfide; Boron nitride; Fracture toughness; Thermal stability; Microhardness; Fracture surface morphology.

OPEN ACCESS

Citation: Rao, Y. S., Shivamurthy, B., Mohan, N. S., Shetty, N., Influence of hBN and MoS2 fillers on toughness and thermal stability of carbon fabric-epoxy composites, Frattura ed Integrità Strutturale, 62 (2022) 240-260.

Received: 12.08.2022
Accepted: 27.08.2022
Online first: 28.08.2022
Published: 01.10.2022

Introduction

Carbon fiber-reinforced epoxy composite (CFREC) is used in aeronautical, railways, automobile, and sports sectors due to its attractive properties [1]. It is used for highly reliable aerospace parts such as wings, tail, and skin panels. Also, used for rocket motors casing and pressure vessels in space applications [2,3]. It is one of the replacements for metals in marine engineering and is used as stiffeners for civil structures and wind turbine blades [4–6]. Due to low shrinkage, chemical inert, heat resistance, easy processability, better impregnation and adhesion properties epoxy is a popular matrix material [7–9]. Its low viscosity at moderate temperature compared to thermoplastics causes uniform spread across the intralayer and interlayer reinforcements [10]. However, its high cross-linking ability develops a three-dimensional

network and leads to high brittleness, low toughness and crack resistance which are the limitation for structural application [11–13]. In addition to this, the interlaminar fracture is the major threatening failure in multi-layered CFREC [14–16].
The toughness is a matrix dominating property in polymer composites. However, the toughness of fiber-reinforced epoxy composite is higher as compared to neat epoxy due to energy consumed for debonding and fiber pullout mechanism before failure [17,18]. Also, reinforced fiber deflects the path of an originated crack and restricts the matrix deformation and imparts toughness to the resultant composite [19]. The intra-ply interaction and the undulations of the woven fabric-reinforced composite tend to bridge the delaminated crack and add considerable resistance to crack propagation as compared to the unidirectional fiber-reinforced composite [20,21]. Also easily process ability, possible to make complex geometries, and good interlaminar fracture resistance as compared to unidirectional fiber-reinforced epoxy composite enhanced the woven fabric-reinforced epoxy composites usage for structural applications [21,22]. The multi-direction of fibers in inter-ply reinforcement showed better toughness compared to the unidirectional fiber orientation in composite [23]. The chemical inertness, non-polar structures and smooth graphite of carbon fiber surface lead to low interlaminar fracture toughness and interlaminar shear strength (ILSS) of CFREC [24,25]. The Z-pinning, through-thickness stitching and 3D braiding/weaving also improve fracture toughness. However, the stated approaches are not economical due to the high production cost and sacrifice the in-plane mechanical properties due to in-plane fiber volume loss [26]. The fracture modes in fiber-reinforced polymer (FRP) are crack opening tensile mode (mode-I), shear mode (mode-II), tearing mode (mode-III) and mixed-mode [20]. The resistance exhibited by a material against these fracture modes is quantified through fracture toughness. Stress intensity factor (K_C) is one such quantitative variable signifying material toughness. The threshold value of K_C indicates the maximum value of stress that a specimen containing a crack can withstand before fracture [27].
The carbonaceous materials like graphene nanoplatelets (GNPs) [9,28,29], carbon nanotubes (CNTs) [28–31], carbon nanofibers (CNFs) [23,32], and carbon blacks (CBs) [29] are used as reinforcement to enhance the toughness of neat epoxy/carbon fiber-epoxy/glass fiber-epoxy composites. Also, the fracture toughness of epoxy-based composite reinforced with filler such as clay [33], aluminium oxide (Al_2O_3) [34], titanium dioxide (TiO_2) [34,35], glass fibers [36], and silica (SiO_2) [36] were demonstrated in the literature. Improving the fracture toughness balanced with other thermomechanical properties (stiffness, strength, glass transition temperature (Tg) etc.) of CFREC is a challenge.
A derivative of graphene such as GNPs and graphene oxide (GO) used as a filler in epoxy to improve toughness [37]. The GNPs in epoxy enhance the toughness due to bridging the crack faces, crack pinning and mechanical locking. The wrinkled structure and large surface area of GNPs improved adhesion with epoxy resin which exhibits crack deflection and hinders the crack path in both the matrix and fiber-matrix interface [38]. The rigid nature of GNPs and CNTs deflect the cracks in an epoxy matrix [39]. The functional groups like OH and COOH at the surface of GO form hydrogen bonding with the epoxide groups resulting in better intermolecular interactions and improved toughness [40]. The functionalized GNPs contained oxygen functional groups bond with the epoxy group and enhanced the toughness [9]. However, a higher concentration of functionalized GNPs in epoxy leads to ineffective cross-linking. The amino functionalized CNTs in epoxy improved the interfacial adhesion with epoxy and leads to improved toughness [30]. This is attributed to good dispersion, large aspect ratio and specific surface area of CNTs. The nucleation of voids, crack deflection, and epoxy deformation are decisive factors in toughness improvement of amino functionalized CNTs filled epoxy. Shirodkar et al. [28] reported multi-walled carbon nanotubes (MWCNTs) reinforced epoxy composite showed higher toughness than GNPs and hybrid filler (MWCNTs and GNPs) reinforced epoxy composites. This is due to a greater number of MWCNTs reinforcement than GNPs for the same wt.%, and also due to the MWCNTs lengthwise structure cause mechanical interlocking and crack bridging effectively as compared to GNPs. Most of the microscopic analysis of fractured CNTs reinforced epoxy composites showed rougher fracture surface which confirm the crack path deflection and obstruction by the CNTs. Also, the CNTs pullout, CNTs rupture, crack pinning and crack tip blunting are the common toughening mechanisms reported in CNTs reinforced epoxy composite [17,41,42]. The CNFs also improve toughness of epoxy composite due to twisting and spreading of the coiled graphitic sheets in the matrix [32].
In addition to above said carbonaceous fillers, nanoclay and ceramic fillers are also used for epoxy toughening. The alkylammonium treated clay increased the toughness of epoxy and slightly decreased Tg of the composite [33]. Hussain et al. [35] showed that micron-size TiO_2 dispersed epoxy improved toughness compared to same nano fillers. Jajam and Tippur [36] reported nano SiO_2 is an effective epoxy toughening filler compared to micro-glass particulates due to higher interfacial surface area and effective SiO_2-epoxy interfacial contact. The Al_2O_3 particle also enhances toughness of epoxy through obstruct and deflects crack, further creates into micro-cracks and debonding particles which consume energy [34].
The toughness of fabric/fiber reinforced composites study is important for structural application. The toughness improvement in CFREC was related to stronger carbon fiber/filler/epoxy interactions that bridge the crack interface and impart resistance for crack propagation. Borowski et al. [31] showed MWCNTs and carbon fibers bridging at the crack tip

improve the toughness of CFREC. GNPs and CNFs in CFREC significantly improved mode-I toughness and MWCNTs loaded CFREC improved mode-II toughness of composite [23,29,31]. Tab. 1 represents the toughness of various filler loaded epoxy and fiber-reinforced epoxy composites.

The long and short-chain molecules are bonded by weak Van-Der-Waals force in most of the polymer matrix causing easy degradation under heating and restricts elevated operating temperature application [43]. The thermal stability of polymer can be improved by incorporating a judicious quantity of suitable fillers [44,45]. The hexagonal boron nitride (hBN) filler gained significant attention due to its excellent thermal conductivity, thermal stability apart from its non-abrasive nature and high modulus [46,47]. BN efficient than CNFs because of the high bonding potentials of B and N atoms, the polarized nature of B-N bonding, accompanied by coulomb and Van-Der-Waals force of interactions between boron nitride and polymer matrix. This is due to the partial ionic structure of B-N [48]. Thermogravimetric analysis of polymer composites showed improved degradation temperature due to the addition of hBN [49,50]. The hBN filler improved thermal stability of epoxy-based composite [50] and polyether ketone-based composite [49] due to the restriction of molecular movement and better interaction between polymer molecules and filler surface. The microhardness of polymer composite is increased due to the addition of hBN. It is found that the nano hBN effectively enhanced the microhardness due to less interparticle distance as compared to micro hBN particles in the polymer [51,52]. The addition of molybdenum disulfide (MoS_2) enhances the Tg of epoxy due to the restriction of movement of molecules [53].

From the literature, it is noticed that the toughness of filler loaded CFREC is critically influenced by volume fraction, shape, size and properties of fiber, filler, and matrix in addition to process method and treatment to reinforcement. Hence, the fracture toughness is case-specific. The filler having excellent elastic moduli and strength exhibit increased resistance against crack propagation and are beneficial for improving the composite toughness. The crack branching, crack pinning, filler-debonding, filler pullout, filler bridging and filler-fracture are the various toughening mechanisms observed in the filler dispersed CFREC. Developing a composite of higher toughness and thermal stability without sacrificing other important thermomechanical properties is a challenging task. The present work deals about hBN and MoS_2 filler influence on toughness, microhardness, and thermal stability of carbon fabric-reinforced epoxy composite (CFREC). The mode-I and mixed-mode I/II toughness behavior of the filler loaded CFREC were studied. The fracture surface morphology of the fractured samples was examined to understand the failure mechanism. The research work also focused on the microhardness and thermal mass stability evaluation of the composites.

Composition	Filler		Fracture toughness & % improvement compared to control sample			
	Size	Concentration (wt.%)	K_{IC} (MPa.m$^{1/2}$)	G_{IC} (J.m^{-2})	G_{IIC} (J.m^{-2})	Ref.
GNPs/E, GNPs/CNTs/E	GNPs d: 25 µm, t: 7 nm. CNTs d: 5–15 nm, l: 25 µm.	0.5, 1, 2, 3	1.46 @3% GNPs (89%↑) 1.35 @1.7% GNPs +0.3%CNTs (75%↑)	-	-	Ahmadi-Moghadam and Taheri [39]
EG/E, GO/E, EG/GO/E	Graphite d: 500 µm.	0.25, 0.5, 0.75, 1	1.56 @0.5% EG/GO (64%↑)	6410 @0.5% EG/GO (150%↑)	-	Kang et al. [40]
Pf-GNPs/E	d: 1–3 µm, t< 50 nm.	0.1, 0.25, 0.5, 0.75, 1	0.83 @0.25% Pf-GNPs (22%↑)	245 @0.25% Pf-GNPs (51%↑)	-	Domun et al. [9]
Af-DWCNTs/E	d: 2.8 nm, l≈ 1 µm.	0.1, 0.3, 0.5	0.93 @0.5% Af-DWCNTs (43%↑)	-	-	Gojny et al. [30]
MWCNTs/E, GNPs/E, MWCNTs/GNPs/E	MWCNTs Od: 15 nm, Id: 7 nm, l: 3 µm. GNPs d: 5 µm, t: 15 nm.	0.1, 0.5	1.64 @0.5% MWCNTs (118%↑) 1.58 @0.5% GNPs (110%↑) 1.55 @0.25% MWCNTs/GNPs (106%↑)	1017 @0.5% MWCNTs (311%↑) 923 @0.5% GNPs (273%↑) 927 @0.25% MWCNTs/GNPs (275%↑)	-	Shirodkar et al. [28]

CNFs/E	d: 60–200 nm, l: 30–100 mm.	1, 2, 3	6.6 @2% CNFs (27%↑)	-	-	Zhou et al. [32]
Clay/E	Nano size.	1, 2, 3	0.93 @3% clay (19%↑)	320 @3% clay (36%↑)	-	Bashar et al. [33]
Micro TiO_2/E, Nano TiO_2/E	1 μm and 20 nm.	2.5 to 10* (steps of 2.5)	2.2 @10% micro TiO_2 (83%↑) 1.62 @10% nano TiO_2 (36%↑)	-	-	Hussain et al. [35]
Al_2O_3/E, TiO_2/E	Al_2O_3 13 nm. TiO_2 300 nm.	1 to 10* (steps of 1)	1.10 @10% Al_2O_3 (120%↑) 0.84 @10% TiO_2 (68%↑)	377 @10% Al_2O_3 (360%↑) 172 @10% TiO_2 (110%↑)	-	Wetzel et al. [34]
SiO_2/E, Glass/E	SiO_2 d: 20 nm. Glass d: 35 μm.	3, 5, 7, 10*	5.22 @10% SiO_2 (171%↑) 2.95 @10% glass (53%↑)	-	-	Jajam and Tippur [36]
CFF/GNPs/E	d: 5 μm, t: 6–8 nm.	0.2	18.38 @0.2% GNPs (35%↑)	1660 @0.2% GNPs (38%↑)	-	Jain et al. [38]
CF/Cf-MWCNTs/E	Od: 20–30 nm, Id: 5–10 nm, l: 10–30 μm.	0.5, 1, 1.5	-	1170 @0.5% Cf-MWCNTs (25%↑)	-	Borowski et al. [31]
CFF/GNPs/E, CFF/MWCNTs/E CFF/CBs/E	GNPs Lateral size: 40 μm, t: 10 nm. MWCNTs d: 9.5 nm l: 1.5 μm. CBs d: 240–320 nm.	3	-	2133 @3% GNPs (153%↑) 1511 @3% MWCNTs (79%↑) 491 @3% CBs (42%↓)	346 @3% MWCNTs (115%↑) 229 @3% GNPs (43%↑) 92 @3% CBs (43%↓)	Srivastava et al. [29]
UD-CF/CNFs/E, QI-CF/CNFs/E	d: 20–200 nm, l: 1–6 μm.	0.69, 2	-	172 @0.69% CNFs (9%↑) 148 @0.69% CNFs (23%↑)	-	Palmeri et al. [23]
CFF/hBN/E, CFF/MoS_2/E	hBN 52–201 nm. MoS_2 144–642 nm.	2, 4, 6, 8	23.62 @6% MoS_2 (65.15%↑) 22.09 @6% hBN (54.51%↑)	-	-	Present work

Notes: Af-Amino functionalized; CF-Carbon fiber; CFF-Carbon fiber fabric; Cf-Carboxyl functionalized; d-Diameter; DWCNTs-Double walled carbon nanotubes; E-Epoxy; EG-Expanded graphite; Id-Inner diameter; l-Length; Od-Outer diameter; Pf-Plasma functionalized; QI-Quasi isotropic; t-Thickness; UD-Unidirectional; G_{IC}-mode-I strain energy release rate; G_{IIC}- mode-II strain energy release rate. * denotes Vol.%.

Table 1: Material combination and toughness of various filler loaded epoxy composites.

MATERIALS AND METHODS

Materials

The 2D twill weaved carbon fabric T300-grade and hBN and MoS_2 fillers are used as reinforcements. The epoxy resin (Lapox L12) and the tri-ethylene tetraamine (Lapox K6) hardener were used as matrix. The specification and properties of constituents are mentioned in Tab. 2.

Characterization and testing

The hBN and MoS_2 fillers morphology was investigated using high-resolution transmission electron microscope (HRTEM) (Make/Model: JEOL, JEM-2100, Japan). Carbon fabric-reinforced epoxy composites (with and without filler) laminates were manufactured by hand lay-up and vacuum bag molding process. The interaction of reinforcement and matrix in the composites was studied using Fourier-transform infrared (FTIR) spectrophotometer (Make: Thermo-Scientific Ltd., USA). The fracture toughness was estimated as per three-point bending method (Make: Zwick/Roell, Germany) at a displacement rate of 0.4 mm.min^{-1} in accordance with ASTM D5045 [54] and ASTM E1820 [55]. Scanning electron microscope (SEM) (Make: JEOL, JSM-6380LA, Japan) was used to investigate the fracture surface morphology. The surface hardness was determined using a Matsuzawa microhardness tester. The thermal stability of composites was investigated through thermogravimetric (TG) curves obtained by thermogravimetric analyzer (TGA) (Make/Model: PerkinElmer TGA-4000, USA) in a nitrogen gas atmosphere (flow rate 30 ml.min^{-1}).

Carbon fabric		Matrix		Fillers	hBN	MoS_2
Area density	200 g.m^{-2}	Epoxy resin (Lapox L12)		Density (g.cm^{-3})	2.1	5.1
Threads/cm	5	Epoxy value	5.35 Eq. kg^{-1}	Young's modulus (GPa)	925	359
Thickness	0.30 mm	Viscosity @ 25 °C	10500 mPa.s	Bulk modulus (GPa)	36	55
Yarn	200 tex	Volatile content @ 105 °C /Hr.	0.4 %	Melting point (°C)	2973	1185
Fiber diameter	7 µm			Mohs hardness	1-2	1-1.5
Fiber density	1.8 g.cm^{-3}	Hardener (Lapox K6)				
Fiber strength	5089 MPa	Viscosity @ 25 °C	10 mPa.s			
Modulus	205 GPa	Pot life @ 80 °C	60 min			
Conductivity	498W.m^{-1} K^{-1}	Gel time @ 80 °C	90 min			

Table 2: Specification and properties of constituents of composites.

Fracture toughness estimation

In the present work pure mode-I and mixed-mode I/II toughness behavior is estimated. Toughness test specimen detailed dimensions and loading configuration of (a) mode-I and (b) mixed-mode I/II are shown in Fig. 1. At least three replicate tests were performed for each material combination to account for the statistical variation in the toughness. The test is performed until the specimen completely breaks into two halves to observe fracture surface morphology.

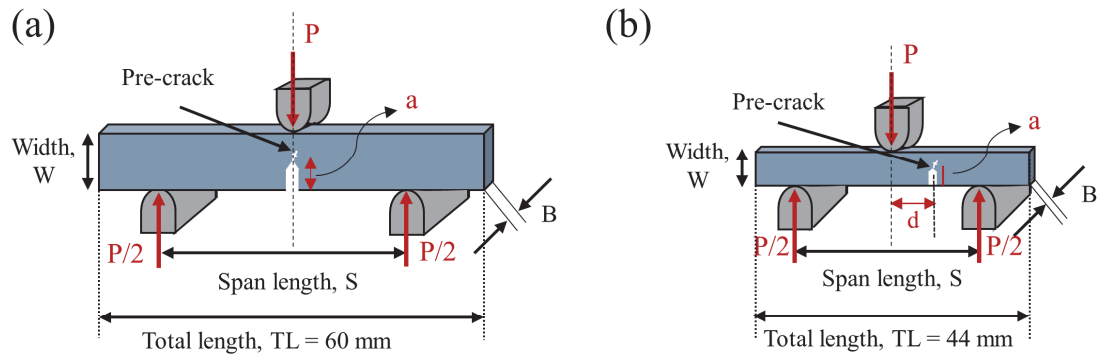

Loading type	S	W	B	a
Pure mode-I	40	9	4	4.5

Loading type	S	W	B	a	d
Mixed-mode I/II	30	6	4	3	6

Figure 1: Toughness test specimen dimensions and loading configuration of (a) mode-I and (b) mixed-mode I/II.

The toughness of each composite specimen K_{IC} as per ASTM D5045 according to pure mode-I loading is estimated using Eqn. (1) [54]. The factor f(a/W) in Eqn. (1) was computed by Eqn. (2) [55,56]. The K_I and K_{II} are the stress intensity components determined as per ASTM E1820 according to the mixed-mode I/II loading by Eqn.s (3) and (4) [55,57]. The values of normalized geometric function F_I and F_{II} are 0.3193 and 0.0715 respectively for the present case is estimated by interpolation based on the value found in the literature [57,58]. The bending stress in Eqns. (3) and (4) was computed by Eqn. (5).

$$K_{IC}=\frac{P_{max}S}{BW^{3/2}}.f\left(\frac{a}{W}\right) \tag{1}$$

$$f\left(\frac{a}{W}\right)=\frac{3\left(\frac{a}{W}\right)^{1/2}\left[1.99-\left(\frac{a}{W}\right)\left(1-\frac{a}{W}\right)\left(2.15-3.93\left(\frac{a}{W}\right)+2.7\left(\frac{a}{W}\right)^{2}\right)\right]}{2\left(1+\frac{2a}{W}\right)\left(1-\frac{a}{W}\right)^{3/2}} \tag{2}$$

$$K_I=\sigma_0 F_I\sqrt{\Pi a} \tag{3}$$

$$K_{II}=\sigma_0 F_{II}\sqrt{\Pi a} \tag{4}$$

$$\sigma_0=\frac{3PS}{2W^2B} \tag{5}$$

Sl.no.	hBN			MoS_2		
	1/D (nm^{-1})	d-spacing (nm)	h k l	1/D (nm^{-1})	d-spacing (nm)	h k l
1	5.90	0.34	(0 0 2)	7.41	0.27	(1 0 1)
2	9.01	0.22	(1 0 0)	8.80	0.23	(0 1 2)
3	9.73	0.21	(1 0 1)	12.68	0.16	(0 1 5)
4	11.18	0.18	(1 0 2)	13.07	0.15	(0 0 9)
5	14.90	0.13	(1 0 4)	14.83	0.13	(1 0 7)
6	16.04	0.12	(1 1 0)	15.95	0.12	(1 1 0)
7	17.04	0.11	(1 1 2)	-	-	-

Table 3: The interplanar spacing of hBN and MoS_2 based on the SAED pattern.

RESULTS AND DISCUSSION

Morphology of fillers

The hBN-ethanol and MoS_2-ethanol homogenously dispersed solution was prepared, and a drop was taken on a carbon-coated copper grid and morphology was studied by the HRTEM. The HRTEM images at various magnifications of hBN and MoS_2 fillers are shown in Fig. 2. It is found that most of the hBN resembles 2D disk and (Fig. 2(a-b)) few of flake type (Fig. 2(c)). The hBN size is between 52-201 nm (Fig. 2(b)) and spacing between the layers is 0.34 nm corresponds to the (002) lattice plane (Fig. 2(d)). The HRTEM images of MoS_2 filler shown in Fig. 2(f-i). It

reveals that the MoS_2 resemble thin sheets with folded edges (Fig. 2(f-h)) and the lateral size is 144-642 nm. Interlayer distance is 0.3 nm corresponds to the (101) lattice plane as shown in Fig. 2(i) [59]. The darker surface in Fig. 2(f-g) indicates overlapping of thin nanosheets. The selective area electron diffraction (SAED) images reveal both fillers of polycrystalline nature. The d-spacings of hBN and MoS_2 filler materials are estimated from the diameter (D) and radius (R) with respect to central spot of SAED images as shown in Fig. 2(e) and 2(j) respectively. The D and R are measured on images using Image-J software. Further, Miller indices values (hkl) were identified by comparing the d-spacing with the Joint committee on powder diffraction standard (JCPDS) value of hBN (card no. 34-0421) and MoS_2 (card no. 89-5112) respectively and are shown in Tab. 3.

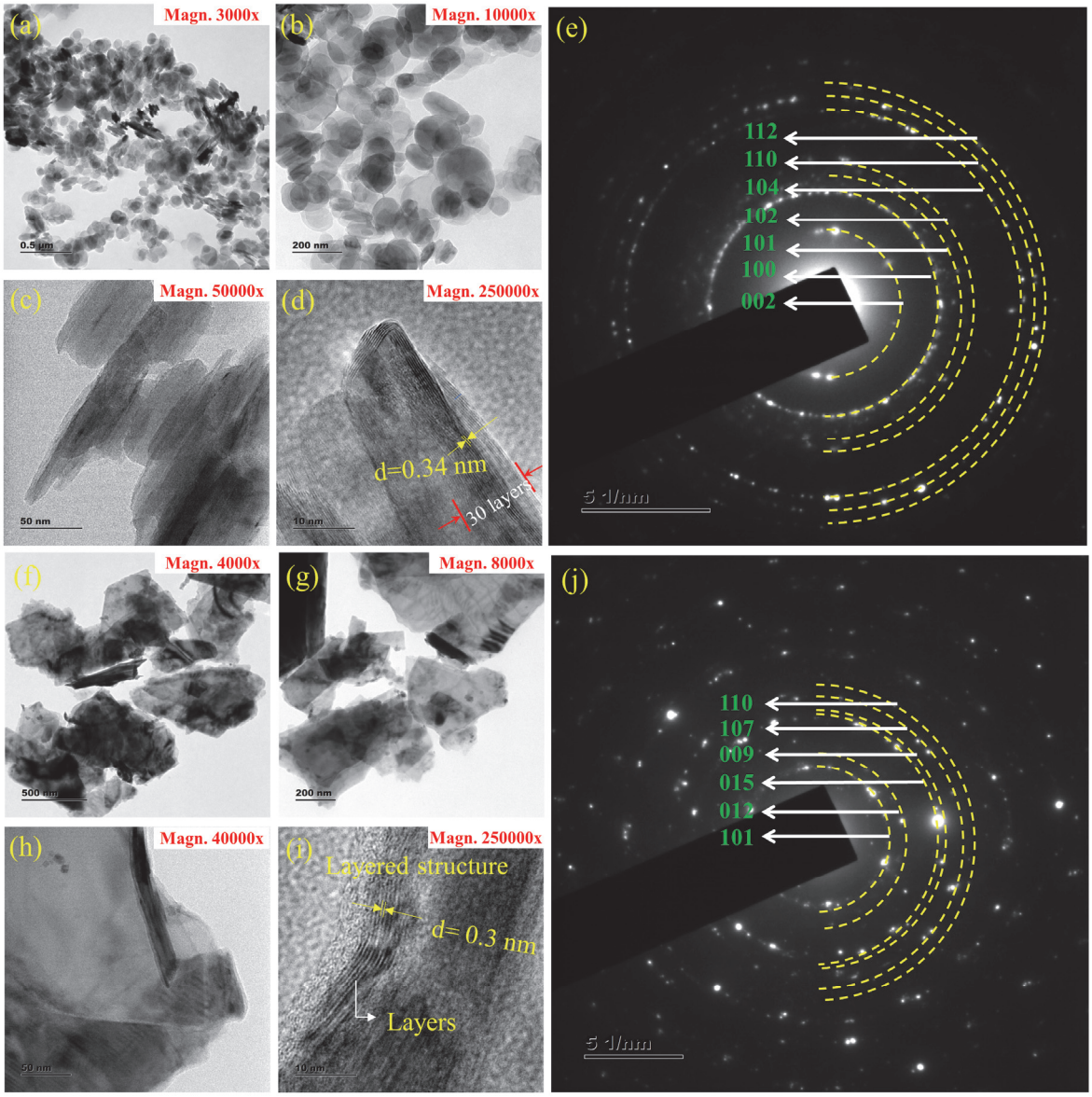

Figure 2: HRTEM images (a-d) hBN morphology, (e) hBN SAED pattern, (f-i) MoS_2 morphology and (j) MoS_2 SAED pattern.

Fabrication of composite laminates

Eight composite laminates were fabricated by using hBN and MoS_2 fillers of 2, 4, 6, and 8 wt.% and carbon fabric as reinforcement in an epoxy matrix. Also, a carbon fabric-reinforced epoxy laminate without filler was fabricated as a control. The constituents of the composites are mentioned in Tab. 4. The pre-determined quantity of filler dispersed in the known quantity of epoxy matrix by magnetic stirring (Make/Model: Remi 5MLH, India) at 500 rpm and temperature of 70 °C.

Further 30 minutes sonication (Make: Q-sonica, USA) was performed at 20 kHz to get homogeneous mix. The high-frequency ultra-sonic waves promote the de-agglomeration of filler. The resultant solution was coated over ten layers of fabrics and filed up one above the other, then the stacked laminate is subjected to the vacuum pressure at 46000 N.m^{-2} for 20 minutes to facilitate the resin flow over the fabric and remove the excess resin if any. The post-curing was performed in a hot-air oven at 75 °C for 90 minutes followed ambient cooling for 24 hours. It is found that the thickness of the fabricated laminates was approximately 4 mm. Toughness test specimens as per dimensions shown in Fig. 1 are prepared from each laminate.

Composite code	Epoxy resin + hardener (wt.%)	Carbon fabric (wt.%)	hBN (wt.%)	MoS_2 (wt.%)
Neat-CFREC	50	50	-	-
2BN-CFREC	48	50	2	-
4BN-CFREC	46	50	4	-
6BN-CFREC	44	50	6	-
8BN-CFREC	42	50	8	-
2MoS_2-CFREC	48	50	-	2
4MoS_2-CFREC	46	50	-	4
6MoS_2-CFREC	44	50	-	6
8MoS_2-CFREC	42	50	-	8

Table 4: Constituents of the composites.

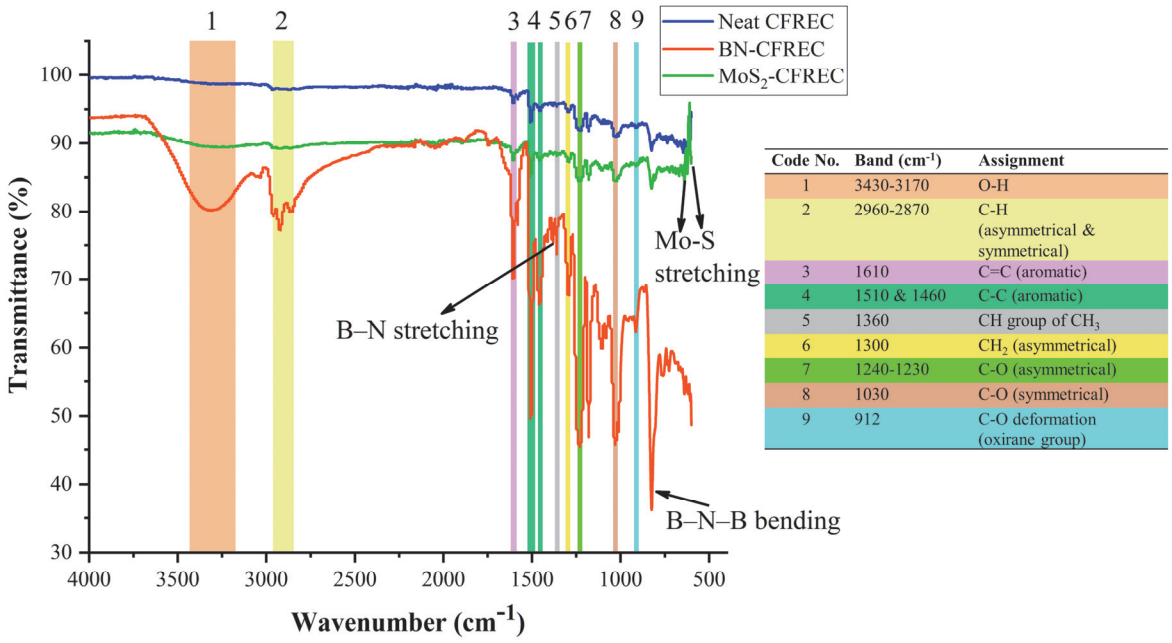

Figure 3: FTIR spectrum of neat CFREC, BN-CFREC and MoS_2-CFREC.

FTIR spectroscopic analysis

Fig. 3 indicates the FTIR spectrum of CFREC with and without filler between wavenumbers 4000 to 600 cm^{-1}. The IR

absorption between 3430 to 3170 cm^{-1} in the FTIR spectra of CFREC confirms the hydroxyl stretch vibration of epoxy. The IR band between 2950 and 2870 cm^{-1} is attributed to the symmetric and asymmetric stretch vibrations of C-H bond respectively. The stretching of C=C aromatic rings is confirmed by the instantaneous descent in the spectrum at 1610 cm^{-1}. The IR absorption at 1510 and 1460 cm^{-1} correspond to stretching of C-C aromatic group. The vibration of C-H group present in CH_3 exhibits IR absorption at 1360 cm^{-1}. The spectra peak at 1300 cm^{-1} corresponds to asymmetrical CH_2 deformation. The asymmetrical and symmetrical aromatic C-O stretching in ethers indicates IR absorption at ring breathing frequency 1230 and 1030 cm^{-1} respectively. The C-O deformation of the oxirane group (epoxy-functional group) was confirmed at 912 cm^{-1}. These are all epoxy related peaks in line with the published literature [60,61]. IR absorption at 1230 cm^{-1} confirms that the active hydrogen group of aromatic nitro compounds open the epoxy rings to form cross-links. The FTIR spectrum of hBN dispersed CFREC indicates two significant IR absorption peaks at 1380 and 823 cm^{-1} corresponding to the rectilinear B–N stretching and out-of-plane B–N–B bending mode, respectively [62]. The hydroxyl and amine functional groups stretching between 3400-3100 cm^{-1} are sharper and enlarged in hBN dispersed CFREC compared to neat CFREC indicating improved cross-link density and hydrogen bonding formation between epoxy molecule and nitrogen atoms [63]. The FTIR spectrum of MoS_2 reinforced CFREC confirms the absorption peaks at 638 and 601 cm^{-1} corresponding to Mo-S stretching [64].

Pure mode-I fracture toughness

The toughness of hBN and MoS_2 filler loaded CFREC are investigated as per mode-I and mixed-mode I/II. The force versus displacement behavior of mode-I test is represented in Fig. 4(a-b). The slope of the force-displacement curve upto peak load as shown in Fig. 4(a-b) indicates the stiffness is increased with an increase of both types of filler content in the composites upto 6 wt.%. Also, found that the peak load is increased with filler content in all the composites upto 6 wt.%. The increased stiffness and toughness are attributed to effective reinforcement of fillers in the matrix. The uniformly dispersed high modulus filler effectively shares load through matrix-filler-fiber. This significantly influences load-carrying capacity. Also, the modification of matrix cross-linking due to the addition of filler affects on deforming behavior of the composites. Further filler loading beyond 6 wt.% deteriorates the stiffness due to agglomeration of fillers. The layered stacking of agglomerated MoS_2 or hBN sheets/disk/flake in the matrix led to frequent slippage and reduced stiffness. This is shown as decreased slope of force-displacement curve upto peak load at higher filler concentration. The slope of force-displacement curve of various composites in the decreasing order is 6BN-CFREC, 6MoS_2-CFREC, 4MoS_2-CFREC≈4BN-CFREC, 8MoS_2-CFREC, 2BN-CFREC, 2MoS_2-CFREC, 8BN-CFREC, and neat-CFREC. However, all the filler loaded CFREC showed higher stiffness than neat CFREC. It indicates filler contributes their stiffness to the matrix of the composites.

The stick-slip pattern is one of the distinct features of the woven fabric-reinforced composite due to the crack-front follows the contour of the fabric surfaces [65]. This is attributed to unstable crack propagation in the composites subjected to loading. The intake load reduces when crack propagates along the fiber direction and rises when the fibers in the fabric obstruct the movement of crack. In the present study, frequently observed sudden load drop and load rise represented as stick-slip (zig-zag) patterns in the force-displacement curve beyond the peak load in all the types of composites. By observing carefully, more frequent, low amplitude, regular and uniform stick-slip pattern is present in 2, 4, 6 wt.% filler loaded CFRECs as compared to neat and 8 wt.% filler loaded CFREC. This pattern is different from neat CFREC and 8 wt.% filler loaded CFREC indicates the filler present in the matrix in between the adjacent fibers restricts/deviates the crack before reaching the next fiber zone in the reinforced fabric of composite. This imparts significant crack resistance to the matrix by the fillers. However, at higher concentrations the agglomerated filler zone acts as stress raiser and toughening effect deteriorates. The K_{IC} of the composites is reported in Tab. 5 and found that K_{IC} increased with hBN and MoS_2 filler concentration upto 6 wt.%. However, the MoS_2 reinforcement showed better results compared to hBN. It is found that addition of 6 wt.% MoS_2 showed 65% improvement in K_{IC} (23.62 $MPa.m^{1/2}$) which is the highest compared to all the composites. The high surface area MoS_2 compared to hBN filler [66] leads to better interaction with matrix, arrest the propagation of crack smoothly is responsible for better K_{IC} of MoS_2-CFREC compared to BN-CFREC.

The crack path deflection around the fiber, crack bowing, fiber pullout, fiber bridging and fiber debonding from the matrix are the toughening mechanisms in FRP composites reported in literature. Void formation around the filler and debonding, pullout, and rupture of filler are the toughening mechanism of filler loaded polymer composites [17,33,67]. In addition to above filler stretching, bridging and restriction/deflection of cracks path by the filler obstruction are also reported as toughening mechanisms in filler loaded composites [34,68].

In the present investigation, the toughening mechanism is in line with the literature. The morphology of fractured surface of CFREC with and without filler is shown in Fig. 5(a-i) and 6(a-c). In the case of neat CFREC, the crack developed in the

matrix and propagates in the direction of fiber along the interface [69] leads to fiber dislodgement and found shear cusps in the matrix demonstrate a brittle failure as shown in Fig. 5(a). The multiple cracks developed in the matrix join each other and dislodged the matrix around the fibers as noticed in Fig. 5(b). The matrix damage due to severe brittle fracture around the fibers and found disintegrated fibers from the matrix as shown in Fig. 5(c). This morphological result supports the lowest K_{IC} in neat CFREC.

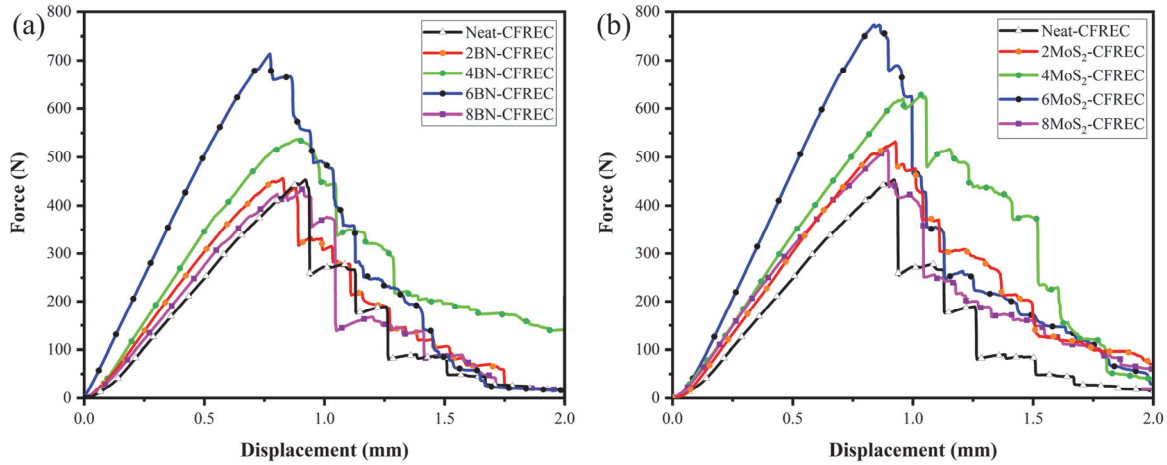

Figure 4: (a-b) Force versus displacement curve of neat CFREC, BN-CFREC and MoS_2-CFREC tested in mode-I loading.

Composite samples	Mode-I			Mixed-mode I/II				
	Pmax (N) Average (Standard error)	K_{IC} (Mpa.m$^{1/2}$)	Gain K_{IC} (%)	Pmax (N) Average (Standard error)	Peak stress (σ_0) (MPa)	K_I (Mpa.m$^{1/2}$)	K_{II} (Mpa.m$^{1/2}$)	Gain K_I, K_{II} (%)
Neat CFREC	458.55 (5.36)	14.30	-	371.68 (8.39)	116.15	3.60	0.81	-
2BN-CFREC	460.78 (4.65)	14.37	0.48	501.75 (5.79)	156.80	4.86	1.09	34.99
4BN-CFREC	521.65 (15.52)	16.27	13.76	580.95 (6.27)	181.55	5.63	1.26	56.30
6BN-CFREC	708.50 (5.50)	22.09	54.51	745.01 (4.96)	232.82	7.22	1.62	100.50
8BN-CFREC	443.47 (9.80)	13.83	-3.28	468.65 (6.15)	146.45	4.54	1.02	26.09
2MoS_2-CFREC	516.69 (15.49)	16.11	12.68	438.34 (4.06)	136.98	4.25	0.95	17.93
4MoS_2-CFREC	629.02 (0.33)	19.62	37.17	593.58 (19.60)	185.50	5.75	1.29	59.70
6MoS_2-CFREC	757.30 (15.74)	23.62	65.15	564.41 (22.91)	176.38	5.47	1.22	51.85
8MoS_2-CFREC	521.60 (4.71)	16.27	13.75	491.60 (3.01)	153.63	4.76	1.07	32.22

Table 5: Mode-I and mixed-mode I/II toughness test results of neat and filler loaded CFREC.

The fractured morphology of 6MoS_2-CFREC is shown in Fig. 5(d) reveals improved integrity of fiber and matrix as compared to neat CFREC Fig. 5(a). The interfacial bonding between fiber, matrix, and filler of 6MoS_2-CFREC as shown in Fig. 5(e) and carbon fiber failure and pullout imprints as shown in Fig. 5(f) due to enhanced matrix toughness is noticed. This mechanism demands more energy to fracture than neat CFREC. Fig. 5(g-i) represents the fracture surface morphology of 6BN-CFREC. It is found shear and bending of carbon fibers along the crack propagation direction as observed in Fig. 5(g). The micro-voids shown in Fig. 5(h) act as a crack resisting zone because significant energy is needed for a crack to propagate further. In addition to this observed obstruction to the crack propagation by hBN particles in the matrix is shown in Fig. 5(i). As discussed earlier the filler agglomeration in 8BN-CFREC leads to poor wetting of filler and is separated from the matrix observed as shown in Fig. 6(a). The agglomerated hBN indicates a region of poor structural property which

deteriorates effective load transfer from the matrix to the reinforcement. As a result, the carbon fiber-epoxy interface bond is disrupted at a few locations as shown in Fig. 6(b-c).

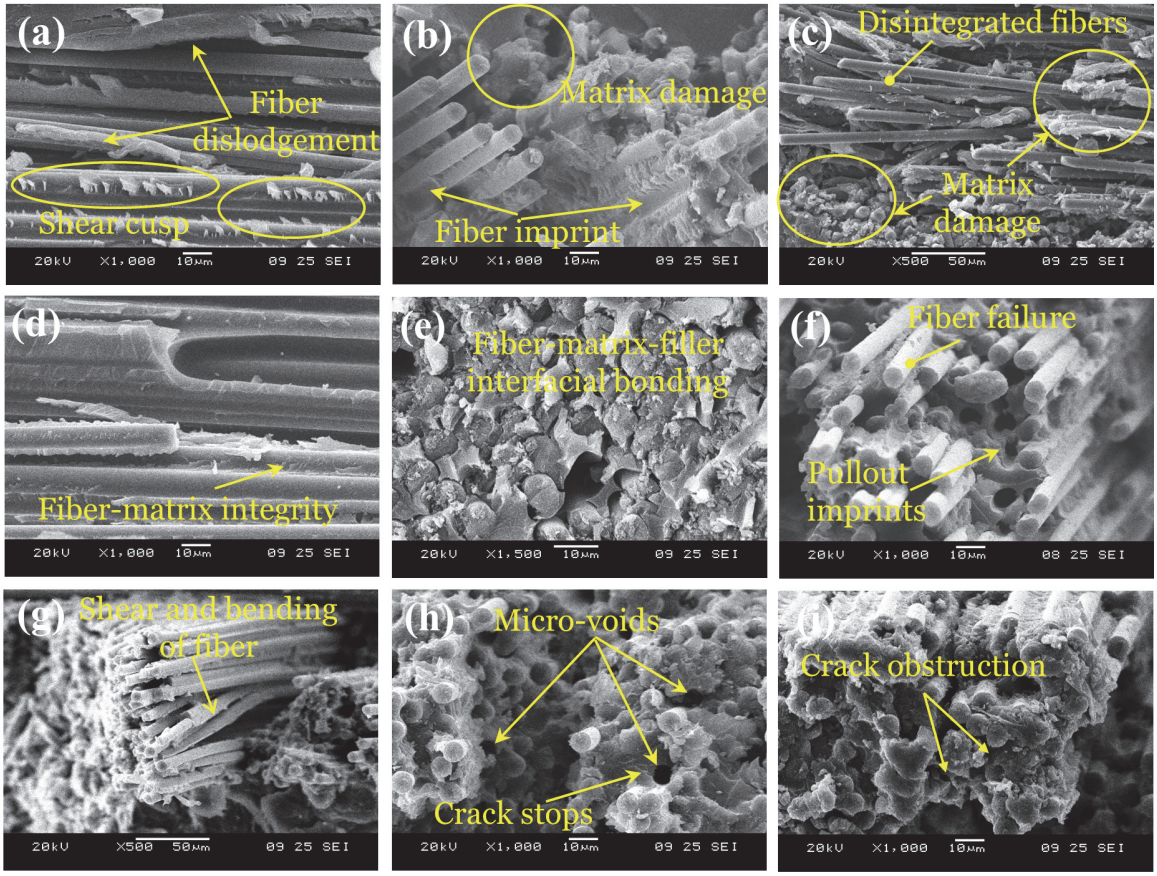

Figure 5: Mode-I type toughness test specimen fractured surface morphology: (a-c) neat CFREC, (d-f) 6MoS_2-CFREC and (g-i) 6BN-CFREC.

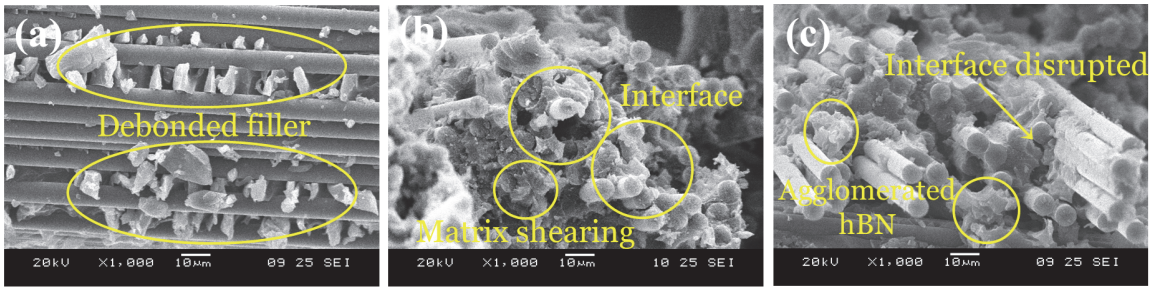

Figure 6: Mode-I type toughness test specimen fractured surface morphology: (a-c) 8BN-CFREC.

Mixed-mode I/II fracture toughness

The force versus displacement behavior of mixed-mode I/II test is represented in Fig. 7(a-b). The stiffness and peak load increased with an increase of hBN filler content up to 6 wt.% and found it is highest in hBN filler loaded CFREC as shown in Fig. 7(a). This is attributed to higher stiffness of hBN filler compared to MoS_2. The increasing trend of stiffness and peak load also observed due to the addition of MoS_2 filler loading. However, the maximum stiffness and peak load were obtained at 4 wt.% MoS_2 filler loading and beyond 4 wt.% gradually reduce the stiffness and peak load of the composites as shown in Fig. 7(b). This is attributed to low coefficient of friction of MoS_2 layered stacking sheets that slips easily in the matrix and reduced the stiffness. It is found that a significant difference in peak load and stiffness between 4 and 6 wt.% hBN filler

loading compared to the difference in peak load and stiffness between similar quantities of MoS_2 filler loaded composites. This is attributed due to the shape of filler. The disk shape of hBN gives more mechanical interlocking compared to sheet morphology of MoS_2 [64]. Further, agglomeration at 8 wt.% filler loading decreased the stiffness and found slightly higher than neat CFREC.

The frequency of stick-slip patterns beyond peak load observed in mixed-mode loading is less than mode-I. It indicates the hindrances to crack propagation is less compared to mode-I. This is attributed that filler aligned along the loading direction is ineffective to resist crack as in mixed-mode I/II loading. Also noticed from Fig. 7(a-b) the lower stick-slip frequency in neat CFREC. The abrupt load drops beyond the peak value in $8MoS_2$-CFREC attributed to slips of MoS_2 sheets, stress concentrated zones due to agglomeration and brittleness of composite.

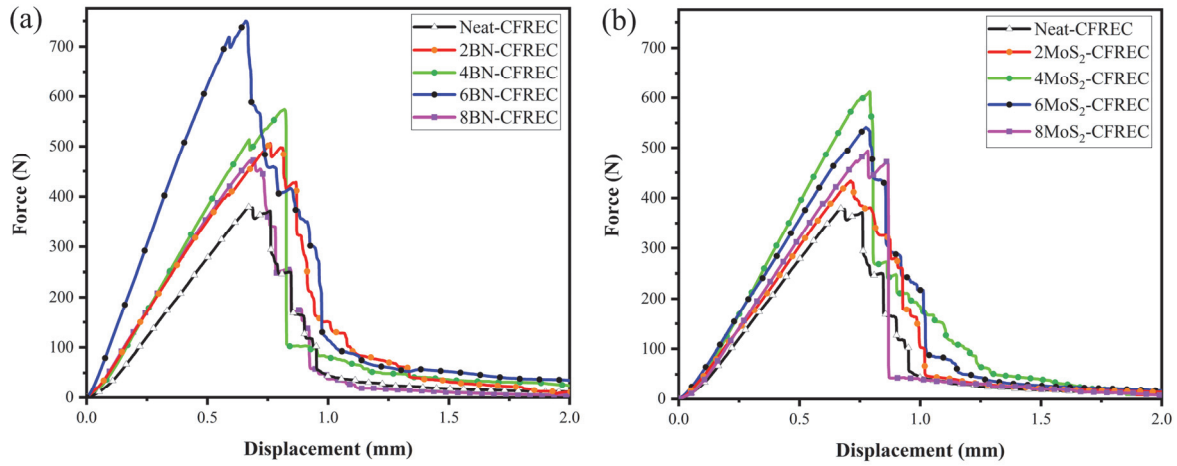

Figure 7: (a-b) Force versus displacement curve of neat CFREC, BN-CFREC and MoS_2-CFREC tested in mixed-mode I/II loading.

The mode-I average stress intensity factor (K_I) caused by normal tensile load and mode-II average stress intensity factor (K_{II}) caused by in-plane shear load [70] are reported in Tab. 5. In the mixed-mode, the crack propagates primarily in opening mode with some sliding [71]. The 6BN-CFREC showed the maximum K_I (7.22 MPa.m$^{1/2}$) and K_{II} (1.62 MPa.m$^{1/2}$) in case of hBN loaded CFREC. The $4MoS_2$-CFREC and $6MoS_2$-CFREC showed almost similar and higher K_I and K_{II} in case of MoS_2 loaded CFREC. This is attributed due to improved ILSS and tensile properties by adding fillers [66]. The lower K_I (4.54 MPa.m$^{1/2}$) and K_{II} (1.02 MPa.m$^{1/2}$) witnessed for 8BN-CFREC still, it is higher than neat CFREC.

The shear hackles, micro-cracking, shallow cusps and shear deformation are the fracture mechanism reported in the morphology of mixed mode-I/II fractured surfaces [13]. In the present study Fig. 8(a-c) depicts neat CFREC mixed-mode toughness test fractured surfaces. It is found that matrix and fibers shear fracture and shallow cusps at the fracture surface of neat CFREC in Fig. 8(a) and (b) are due to the contribution of mode-II loading [72]. The deep pockets visible in Fig. 8(c) were caused due to pulled out bunch of carbon fibers. The morphology of 6BN-CFREC fractured surface is displayed in Fig. 8(d-f). The carbon fiber pullout was seen in Fig. 8(d) of 6BN-CFREC indicates the inability of a crack to propagate in tough hBN dispersed epoxy. The micro-crack deflected in the matrix via the hackle pattern as shown in Fig. 8(e-f) due to shear deformation. The hackle marking indicates a violent stage of fracture and energy dissipation via deformation [36]. Therefore, in this study, the shear hackles in 6BN-CFREC represent tough composite. Fig. 8(g) indicates an intimate interaction of carbon fiber with MoS_2 dispersed epoxy responsible for higher toughness and the shear deformation lines observed in Fig. 8(h) at the fracture surface of $4MoS_2$-CFREC. The shear fracture leads to dislodgement of fiber evident from the fiber imprints of $4MoS_2$-CFREC as shown in Fig. 8(i).

The fracture morphology of 8BN-CFREC is shown in Fig. 9(a-c). The carbon fiber pullout and fiber imprint is observed in Fig. 9(a) due to weak matrix-fiber interaction. The matrix cracking, carbon fiber debonding in Fig. 9(b) and shear cusps formation in Fig. 9(c) indicate brittle failure of 8BN-CFREC due to low toughness. Filler debonded and appear at the surface as fragments/shards (Fig. 9(c)), this was due to poor matrix-filler interaction. The above fracture mechanism found in surface morphology of the fractured specimen is proof of poor wetting of filler and fiber due to agglomeration which deteriorated K_I and K_{II} of 8BN-CFREC. The morphology of $8MoS_2$-CFREC fracture surface is displayed in Fig. 9(d-f). The carbon fiber free from the matrix indicates severe brittle damage of matrix shown in Fig. 9(d). The failure of matrix due to poor wetting and matrix debris are visible as shown in Fig. 9(e). Also, observed pullout of fiber due to poor matrix

fiber interface which is shown in Fig. 9(f). Hence, K_I and K_{II} of 8MoS_2-CFREC are not significantly improved.

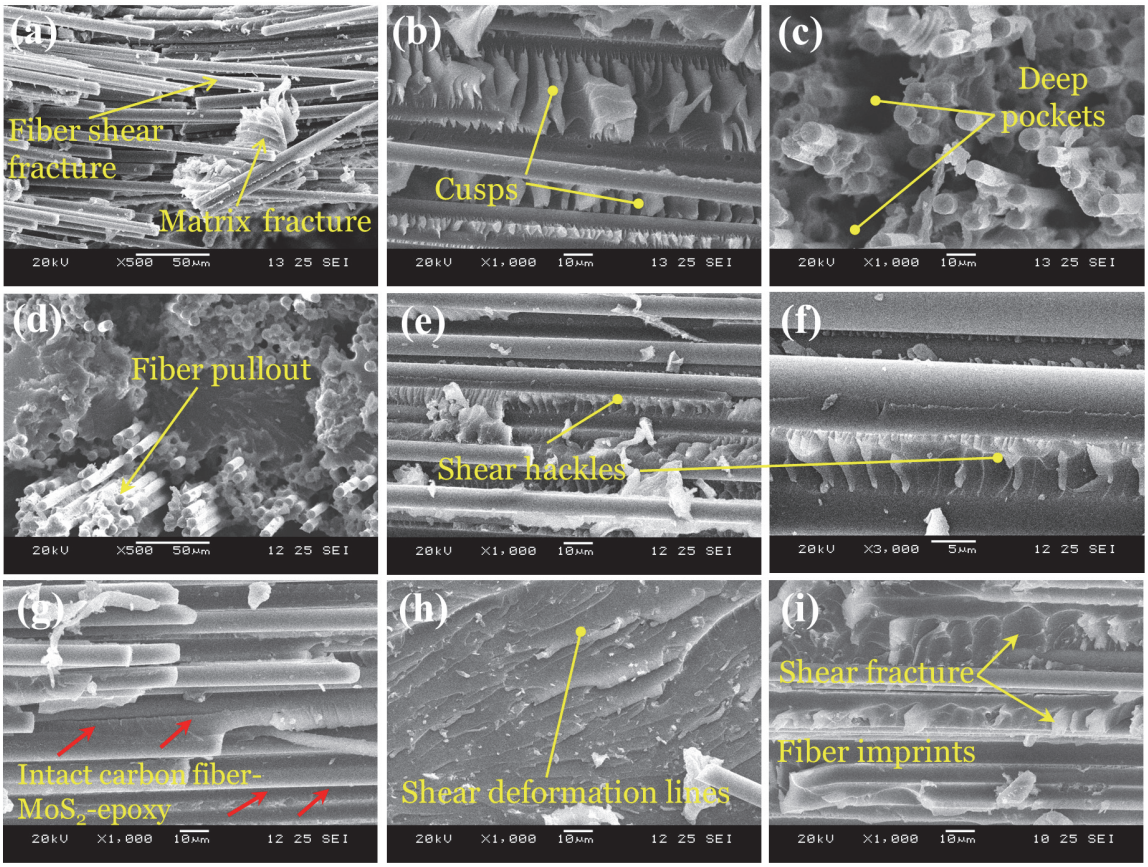

Figure 8: Mixed-mode I/II type toughness test specimen fractured surface morphology: (a-c) neat CFREC, (d-f) 6BN-CFREC and (g-i) 4MoS_2-CFREC.

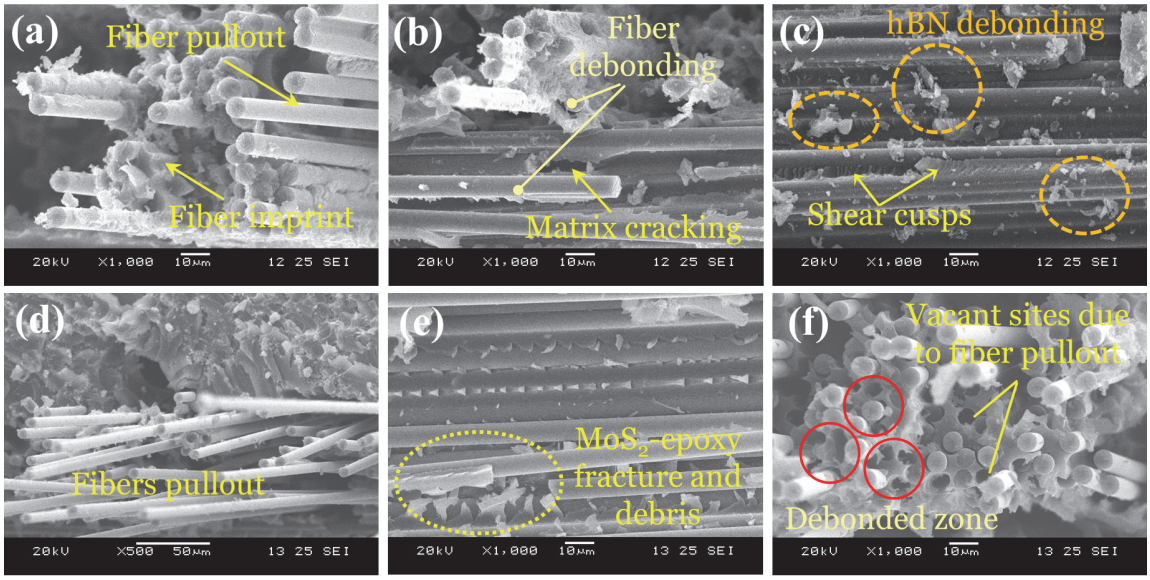

Figure 9: Mixed-mode I/II type toughness test specimen fractured surface morphology: (a-c) 8BN-CFREC and (d-f) 8MoS_2-CFREC.

Microhardness

In the present study, the Vicker's hardness of the composite laminates was studied by applying a 100 g force for 20 seconds on a pyramid-shaped diamond tip indenter placed over the composite surface. Vicker's microhardness versus filler concentration in BN-CFREC and MoS_2-CFREC is plotted in line graph shown in Fig. 10. The microhardness increased with the hBN and MoS_2 fillers upto 6 wt.%. This is attributed that the hBN and MoS_2 uniform dispersion in the matrix alters the cross-linking structure and improved its resistance to deformation through contribution of intrinsic strength and modulus of fillers to the matrix. It is noticed that the microhardness of BN-CFREC is slightly higher than MoS_2-CFREC due to the more stiff and hard nature of hBN compared to MoS_2 [73]. In both types of filler loaded composites, as the filler concentration is increased beyond 6 wt.% microhardness decreased but is still higher than neat CFREC. This decline in microhardness at the higher filler content might be due to the agglomeration and voids in the composite.

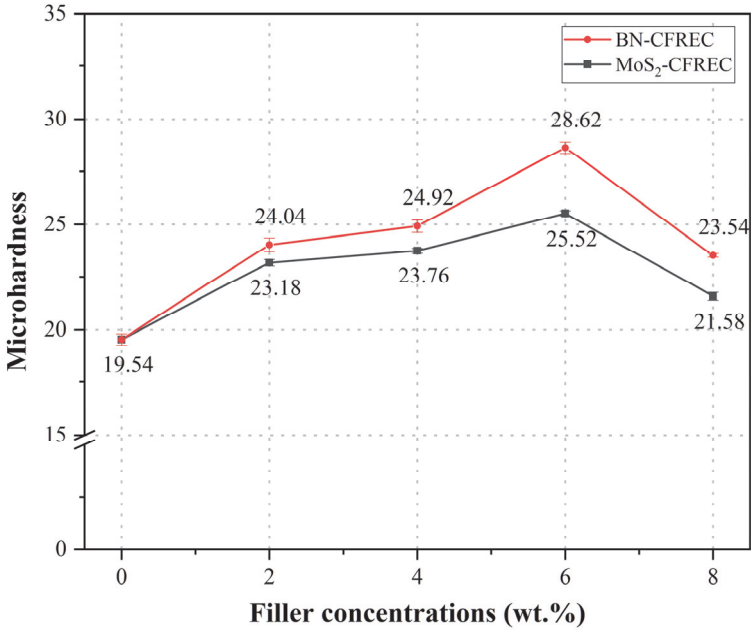

Figure 10: Microhardness versus filler concentration of BN-CFREC and MoS_2-CFREC.

Analysis of thermal stability and decomposition kinetics

Ability of material to maintain its physical integrity and structure properties with minimum deterioration indicates its thermal stability. Composite samples of 10 mg were kept in a crucible of TG analyzer and heated up to 200 °C for 5 minutes to eradicate humidity. Further, the sample was heated to 900 °C at a heating rate of 20 °C min^{-1} in the presence of N_2 gas to avoid carbon oxidation. The weight loss was monitored as the temperature rise and weight loss as a function of temperature for various composites are plotted as shown in Fig. 11(a-b). The initial early weight loss near 200 °C was due to the evaporation of unreacted monomers and other volatile substances [74]. The volatile evolved could be CO_2, H_2O, CO, aliphatic or aromatic compounds [75]. The onset decomposition temperature, transitional temperature $T_{d5\%}$ (correspond to 5% weight loss) and $T_{d25\%}$ (correspond to 25% weight loss) of the composite were measured and presented in Tab. 6. Fig. 11(a-b) reveals the decomposition of the molecular chain of cross-linked epoxy noticed at 300 to 400 °C. However, depending on the precursor and mode of heat treatment used in the synthesis of carbon fiber, the carbon fibers decompose at high temperature between 400 and 1000 °C as per literature [76]. In the present work polyacrylonitrile (PAN) based carbon fabric is used. Hence the decomposition of fibers starts near at 400 °C as shown in Fig. 11(a-b). The addition of filler to the CFREC upgrades the onset degradation temperature as compared to neat CFREC. The neat CFREC exhibits 25% weight loss at 395 °C, the 4MoS_2-CFREC and 4BN-CFREC at 430 and 411 °C respectively.

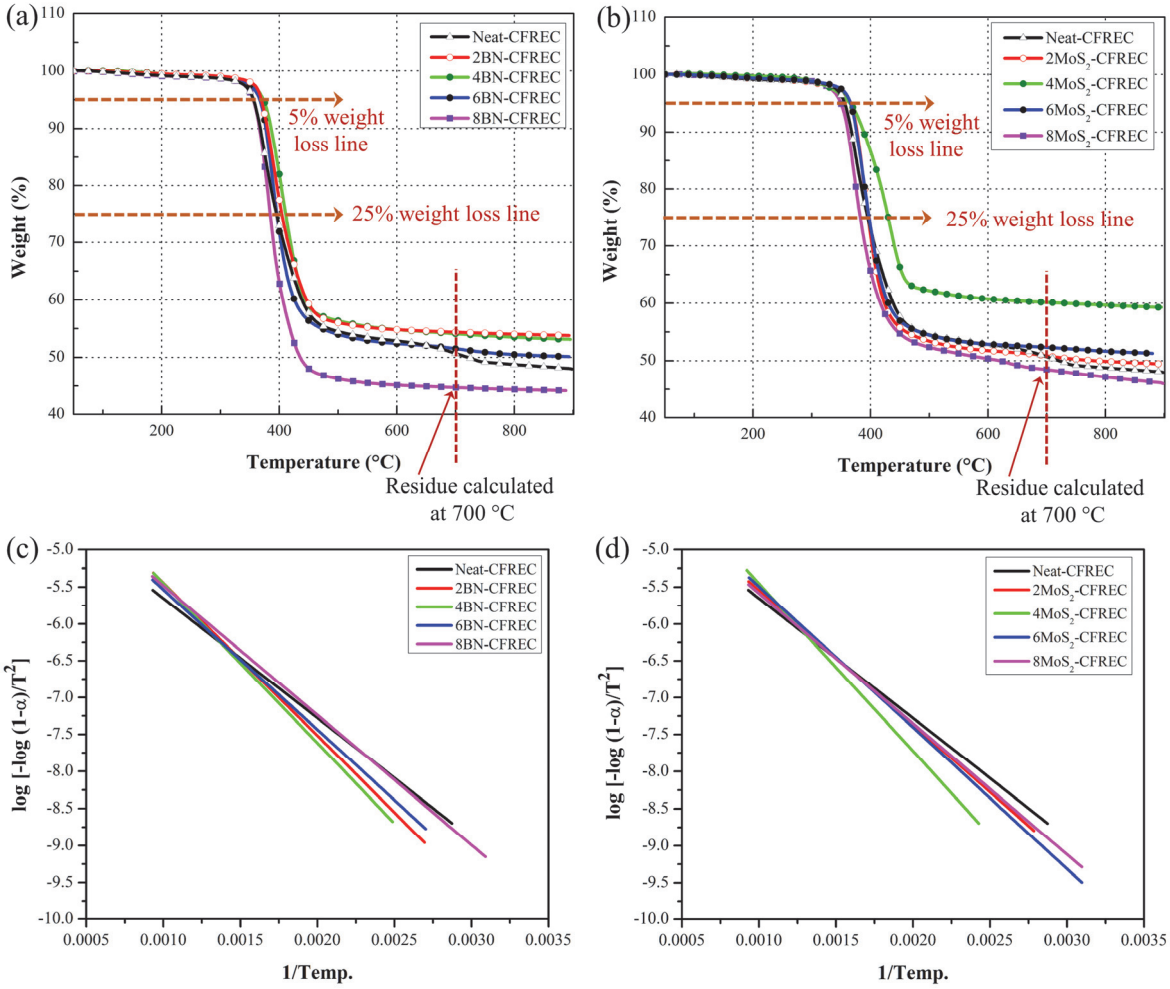

Figure 11: Weight loss versus temperature of (a) BN-CFREC; (b) MoS_2-CFREC; and Coats-Redfern linear graph of (c) BN-CFREC; (d) MoS_2-CFREC.

Composite samples	T_{onset} (°C)	$T_{d5\%}$ (°C)	$T_{d25\%}$ (°C)	Residue at 700 °C (wt.%)	E_a ($J.mol^{-1}$)
Neat-CFREC	351.17	356.00	395.28	50.72	31068.06
2BN-CFREC	367.36	369.48	404.42	54.58	39623.63
4BN-CFREC	372.24	373.14	410.82	54.15	41456.31
6BN-CFREC	365.50	366.74	395.97	51.52	36358.73
8BN-CFREC	354.40	355.78	385.01	44.72	33549.85
2MoS_2-CFREC	367.71	365.60	395.75	50.90	34787.78
4MoS_2-CFREC	361.55	365.60	430.23	60.24	43429.00
6MoS_2-CFREC	361.77	366.06	397.80	52.27	36487.80
8MoS_2-CFREC	351.28	349.62	383.18	48.45	33758.18

Table 6: Decomposition temperature and activation energy of neat and filler loaded CFREC.

The 4MoS_2-CFREC attains the highest thermal stability possibly due to improved interaction of MoS_2 with the epoxy resin which reduces the mobility of epoxy molecular chains. In addition, protective layer formed by the MoS_2 sheets retards heat transfer and exhibits frictional heat reduction (lubricant) characteristics [59]. As a result, 4MoS_2-CFREC requires a higher temperature (threshold energy) to initiate decomposition. Thermal stability also improved upto 4 wt.% hBN incorporation in CFREC. This is attributed to delayed diffusion of the volatile decomposition compounds and formation of carbonaceous char insulate and stabilize the composites [77,78]. Also, due to the impermeable nature of hBN, both volatile gases and oxygen molecules have followed a tortuous diffusion path to pass around uniformly dispersed hBN in epoxy. Thus, the mean free paths of gas diffusion through the hBN dispersed epoxy increased which is responsible for the delay in thermal degradation [43]. Therefore, 2D fillers like hBN, MoS_2 can reduce the diffusion and transmission rate of oxygen and volatile gases within the composite, thus slowing down the thermal decomposition.

At 700 °C, the carbonaceous residue of neat CFREC was 50.72% and it increased to 60.24% for 4MoS_2-CFREC. This increase in the residue was due to the formation of a protective layer by the MoS_2 sheets [59] that retards heat transfer to the underlying material. Similarly, the carbonaceous residue of 2BN-CFREC and 4BN-CFREC were 54.58 and 54.15%, respectively. The increased char yield is accredited to the hBN, which forms dense layer as the composite degrades [49].

While the 8MoS_2-CFREC indicates less thermal stability (rapid decomposition) among MoS_2 dispersed CFREC group. In BN-CFREC, the composite's thermal stability was lowered beyond the 4 wt.% hBN loading because hBN probably catalyzes the matrix decomposition due to improved thermal conductivity [79,80] and the large cluster of filler at higher filler concentration might adversely impact the carbon fiber-hBN filler-epoxy interfacial bonding.

The detailed thermal degradation kinetics of all the prepared composites were studied by computing the activation energy (E_a) using the Coats-Redfern Eqn. (6) [81].

$$\log_{10}\left[\frac{-\log_{10}(1-\alpha)}{T^2}\right]=\log_{10}\frac{AR}{\beta E_a}\left[1-\frac{2RT}{E_a}\right]-\frac{E_a}{2.3RT} \tag{6}$$

The $\log_{10}[-\log_{10}(1-\alpha)/T^2]$ versus (1/T) graph is constructed as shown in Fig. 11(c-d). The Ea was computed using the slope of linear graph and reported in Tab. 6. The Ea of the 4MoS_2-CFREC is 43429 J.mol^{-1} which indicates 39.78% higher than the neat CFREC. The higher activation energy also indicates improved thermal stability. The 4BN-CFREC showed the second-highest activation energy of 41456 J.mol^{-1}. At 8 wt.% filler concentration the Ea started decreasing. However, it was higher than the neat CFREC by 8%.

CONCLUSIONS

The toughness, thermal stability and microhardness of hBN and MoS_2 filler dispersed CFREC laminates and the neat CFREC laminate determined and drawn the following conclusions.

- Successfully prepared the CFREC composites with and without fillers by two-stage mixing and vacuum bag molding process. In the case of mode-I fracture toughness test due to the addition of 6 wt.% MoS_2 filler found 65% improvement in toughness of CFREC. Incorporation of 6 wt.% hBN in CFREC enhanced the mixed-mode I/II fracture toughness nearly two times. Enhanced toughness due to improved structure integrity of filler-polymer-fiber in the composites. The main toughening mechanisms are fiber pullout, debonding of filler/fiber, micro-crack deflection and micro-voids which are in line with the literature. Addition of MoS_2 or hBN beyond 6 wt.% leads to agglomeration and deteriorates the toughness.
- Addition of 4 wt.% MoS_2 or 4 wt.% hBN in CFREC enhanced the decomposition temperature. The MoS_2 presence in epoxy reduces mobility epoxy molecules and retards heat transfer. The impermeable nature of hBN resulted tortuous path to escape volatile gases and oxygen. Also, formation of carbonaceous char insulates and stabilizes the composites increasing the decomposition temperature.
- The uniform filler dispersion in the matrix altering the cross-linking structure and improving its resistance to deformation leads to increased hardness.
- Synergistic toughening effect of hBN and MoS_2 filler loading on CFREC worth to be investigated. Also, advanced filler dispersion technique may be adopted for better results. Further, the effect of fiber orientation in reinforced fabric is also expected to influence toughness. Hence, investigation of filler loaded 3D woven fabric-reinforced

epoxy composite may be required. Design of experiment and finite element analysis is required for further to optimize the filler concentration for better specific structural properties.

NOMENCLATURE

a	initial crack length (mm)
A	pre-exponential term
B	specimen thickness (mm)
E_a	activation energy (J.mol^{-1})
f(a/W)	dimensionless correction factor related to specimen geometry and flaw size
F_I	normalized geometric function corresponding to mode-I
F_{II}	normalized geometric function corresponding to mode-II
K_{IC}	critical mode-I stress intensity factor (MPa.mm$^{1/2}$)
K_I	mode-I component of stress intensity factor (MPa.mm$^{1/2}$)
K_{II}	mode-II component of stress intensity factor (MPa.mm$^{1/2}$)
P	applied load (N)
R	gas constant=8.314 J.mol^{-1} K^{-1}
S	span length between the supports (mm)
T	temperature (°K)
W	specimen width (mm)
W_o	initial sample weight (grams)
W_t	residual sample weight at any temperature "T" (grams)
W_f	final sample weight (grams)
Greek letters	
σ_0	bending stress (MPa)
α	degree of decomposition=(Wo-Wt)/(Wo-Wf)
β	heating rate (°C.min^{-1})

CONFLICT OF INTEREST

The authors have no conflicts of interest.

REFERENCES

[1] Oladele, I.O., Omotosho, T.F., Adediran, A.A. (2020). Polymer-based composites: An indispensable material for present and future applications, International Journal of Polymer Science, 2020, pp. 1–12. DOI: 10.1155/2020/8834518.

[2] Palmer, R.J. (2012). History of composites in aeronautics., Wiley Encyclopedia of Composites, 1st ed., Hoboken, USA, John Wiley & Sons, Inc., pp. 1–40.

[3] Lee, T.H. (2012). Review of the composite materials application to the solid rocket motor cases, Journal of the Korean Society for Composite Materials, 25(3), pp. 82–89. DOI: 10.7234/kscm.2012.25.3.082.

[4] Rubino, F., Nisticò, A., Tucci, F., Carlone, P. (2020). Marine application of fiber reinforced composites: A review, Journal of Marine Science and Engineering, 8(1), p. 26. DOI: 10.3390/jmse8010026.

[5] Ulger, T., Okeil, A.M. (2017). Strengthening by stiffening: Fiber-reinforced plastic configuration effects on behavior of shear-deficient steel beams, Journal of Composites for Construction, 21(4), p. 04017011. DOI: 10.1061/(ASCE)CC.1943-5614.0000788.
[6] Mishnaevsky, L., Branner, K., Petersen, H., Beauson, J., McGugan, M., Sørensen, B. (2017). Materials for wind turbine blades: An overview, Materials, 10(11), p. 1285. DOI: 10.3390/ma10111285.
[7] Dai, Z., Zhang, B., Shi, F., Li, M., Zhang, Z., Gu, Y. (2011). Effect of heat treatment on carbon fiber surface properties and fibers/epoxy interfacial adhesion, Applied Surface Science, 257(20), pp. 8457–8461. DOI: 10.1016/j.apsusc.2011.04.129.
[8] Rana, S., Alagirusamy, R., Joshi, M. (2010). Mechanical behavior of carbon nanofibre-reinforced epoxy composites, Journal of Applied Polymer Science, 118(4), pp. 2276–2283. DOI: 10.1002/app.30861.
[9] Domun, N., Hadavinia, H., Zhang, T., Liaghat, G., Vahid, S., Spacie, C., Paton, K.R., Sainsbury, T. (2017). Improving the fracture toughness properties of epoxy using graphene nanoplatelets at low filler content, Nanocomposites, 3(3), pp. 85–96. DOI: 10.1080/20550324.2017.1365414.
[10] Mazumdar, S. (2001). Composites manufacturing: materials, product, and process engineering, 1st ed., Boca Raton, CRC Press, DOI: 10.1201/9781420041989.
[11] Rahmani, H., Najafi, S.H.M., Saffarzadeh-Matin, S., Ashori, A. (2014). Mechanical properties of carbon fiber/epoxy composites: Effects of number of plies, fiber contents, and angle-ply layers, Polymer Engineering & Science, 54(11), pp. 2676–2682. DOI: 10.1002/pen.23820.
[12] Ulus, H., Şahin, Ö.S., Avcı, A. (2015). Enhancement of flexural and shear properties of carbon fiber/epoxy hybrid nanocomposites by boron nitride nano particles and carbon nano tube modification, Fibers and Polymers, 16(12), pp. 2627–2635. DOI: 10.1007/s12221-015-5603-4.
[13] Domun, N., Paton, K.R., Blackman, B.R.K., Kaboglu, C., Vahid, S., Zhang, T., Dear, J.P., Kinloch, A.J., Hadavinia, H. (2020). On the extent of fracture toughness transfer from 1D/2D nanomodified epoxy matrices to glass fibre composites, Journal of Materials Science, 55(11), pp. 4717–4733. DOI: 10.1007/s10853-019-04340-8.
[14] Rao, Y.S., Mohan, N.S., Shetty, N., Shivamurthy, B. (2019). Drilling and structural property study of multi-layered fiber and fabric reinforced polymer composite - A Review, Materials and Manufacturing Processes, 34(14), pp. 1549–1579. DOI: 10.1080/10426914.2019.1686522.
[15] Savage, G. (2006). Enhancing the exploitation and efficiency of fibre-reinforced composite structures by improvement of interlaminar fracture toughness, Engineering Failure Analysis, 13(2), pp. 198–209. DOI: 10.1016/j.engfailanal.2004.12.047.
[16] Sunil Kumar, B.V., Londe, N.V., Lokesha, M., Vasantha Kumar, S.N., Surendranathan, A.O. (2021). Influence of oxidation on fracture toughness of carbon-carbon composites for high-temperature applications, Frattura Ed Integrità Strutturale, 15(58), pp. 105–113. DOI: 10.3221/IGF-ESIS.58.08.
[17] Mousavi, S.R., Estaji, S., Paydayesh, A., Arjmand, M., Jafari, S.H., Nouranian, S., Khonakdar, H.A. (2022). A review of recent progress in improving the fracture toughness of epoxy-based composites using carbonaceous nanofillers, Polymer Composites, 43(4), pp. 1871–1886. DOI: 10.1002/pc.26518.
[18] Siddique, A., Abid, S., Shafiq, F., Nawab, Y., Wang, H., Shi, B., Saleemi, S., Sun, B. (2021). Mode I fracture toughness of fiber-reinforced polymer composites: A review, Journal of Industrial Textiles, 50(8), pp. 1165–1192. DOI: 10.1177/1528083719858767.
[19] Knops, M., Bögle, C. (2006). Gradual failure in fibre/polymer laminates, Composites Science and Technology, 66(5), pp. 616–625. DOI: 10.1016/j.compscitech.2005.07.044.
[20] Daniel, I. M., Ishai, O. (2006). Engineering mechanics of composite materials, 2nd ed., New York, Oxford University Press.
[21] Zabala, H., Aretxabaleta, L., Castillo, G., Aurrekoetxea, J. (2015). Loading rate dependency on mode I interlaminar fracture toughness of unidirectional and woven carbon fibre epoxy composites, Composite Structures, 121, pp. 75–82. DOI: 10.1016/j.compstruct.2014.11.001.
[22] Espadas-Escalante, J.J., Van Dijk, N.P., Isaksson, P. (2018). The effect of free-edges and layer shifting on intralaminar and interlaminar stresses in woven composites, Composite Structures, 185. DOI: 10.1016/j.compstruct.2017.11.014.
[23] Palmeri, M.J., Putz, K.W., Ramanathan, T., Brinson, L.C. (2011). Multi-scale reinforcement of CFRPs using carbon nanofibers, Compos Sci Technol, 71(2), pp. 79–86. DOI: 10.1016/j.compscitech.2010.10.006.
[24] Ma, L., Wu, L., Cheng, X., Zhuo, D., Weng, Z., Wang, R. (2015). Improving the interlaminar properties of polymer composites using a situ accumulation method to construct the multi-scale reinforcement of carbon nanofibers/carbon fibers, Composites Part A: Applied Science and Manufacturing, 72, pp. 65–74.

DOI: 10.1016/j.compositesa.2015.01.023.
[25] Yao, X., Gao, X., Jiang, J., Xu, C., Deng, C., Wang, J. (2018). Comparison of carbon nanotubes and graphene oxide coated carbon fiber for improving the interfacial properties of carbon fiber/epoxy composites, Composites Part B: Engineering, 132, pp. 170–177. DOI: 10.1016/j.compositesb.2017.09.012.
[26] Mouritz, A.P., Cox, B.N. (2010). A mechanistic interpretation of the comparative in-plane mechanical properties of 3D woven, stitched and pinned composites, Composites Part A: Applied Science and Manufacturing, 41(6), pp. 709–728. DOI: 10.1016/j.compositesa.2010.02.001.
[27] Zhu, X.K., Joyce, J.A. (2012). Review of fracture toughness (G, K, J, CTOD, CTOA) testing and standardization, Engineering Fracture Mechanics, 85, pp. 1–46. DOI: 10.1016/j.engfracmech.2012.02.001.
[28] Shirodkar, N., Cheng, S., Seidel, G.D. (2021). Enhancement of Mode I fracture toughness properties of epoxy reinforced with graphene nanoplatelets and carbon nanotubes, Composites Part B: Engineering, 224, p. 109177. DOI: 10.1016/j.compositesb.2021.109177.
[29] Srivastava, V.K., Gries, T., Veit, D., Quadflieg, T., Mohr, B., Kolloch, M. (2017). Effect of nanomaterial on mode I and mode II interlaminar fracture toughness of woven carbon fabric reinforced polymer composites, Engineering Fracture Mechanics, 180, pp. 73–86. DOI: 10.1016/j.engfracmech.2017.05.030.
[30] Gojny, F., Wichmann, M., Fiedler, B., Schulte, K. (2005). Influence of different carbon nanotubes on the mechanical properties of epoxy matrix composites – A comparative study, Composites Science and Technology, 65(15–16), pp. 2300–2313. DOI: 10.1016/j.compscitech.2005.04.021.
[31] Borowski, E., Soliman, E., Kandil, U., Taha, M. (2015). Interlaminar fracture toughness of CFRP laminates incorporating multi-walled carbon nanotubes, Polymers (Basel), 7(6), pp. 1020–1045. DOI: 10.3390/polym7061020.
[32] Zhou, Y., Jeelani, S., Lacy, T. (2014). Experimental study on the mechanical behavior of carbon/epoxy composites with a carbon nanofiber-modified matrix, Journal of Composite Materials, 48(29), pp. 3659–3672. DOI: 10.1177/0021998313512348.
[33] Bashar, M., Mertiny, P., Sundararaj, U. (2014). Effect of nanocomposite structures on fracture behavior of epoxy-clay nanocomposites prepared by different dispersion methods, Journal of Nanomaterials, 2014, pp. 1–12. DOI: 10.1155/2014/312813.
[34] Wetzel, B., Rosso, P., Haupert, F., Friedrich, K. (2006). Epoxy nanocomposites – fracture and toughening mechanisms, Engineering Fracture Mechanics, 73(16), pp. 2375–2398. DOI: 10.1016/j.engfracmech.2006.05.018.
[35] Hussain, M., Nakahira, A., Nishijima, S., Niihara, K. (1996). Fracture behavior and fracture toughness of particulate filled epoxy composites, Materials Letters, 27(1–2), pp. 21–25. DOI: 10.1016/0167-577X(95)00254-5.
[36] Jajam, K.C., Tippur, H. (2012). Quasi-static and dynamic fracture behavior of particulate polymer composites: A study of nano- vs. micro-size filler and loading-rate effects, Composites Part B: Engineering, 43(8), pp. 3467–3481. DOI: 10.1016/j.compositesb.2012.01.042.
[37] Xue, G., Zhang, B., Sun, M., Zhang, X., Li, J., Wang, L., Song, C. (2019). Morphology, thermal and mechanical properties of epoxy adhesives containing well-dispersed graphene oxide, International Journal of Adhesion and Adhesives, 88, pp. 11–18. DOI: 10.1016/j.ijadhadh.2018.10.011.
[38] Jain, V., Bisht, A., Jaiswal, S., Dasgupta, K., Lahiri, D. (2021). Assessment of interfacial interaction in graphene nanoplatelets and carbon fiber-reinforced epoxy matrix multiscale composites and its effect on mechanical behavior, Journal of Materials Engineering and Performance, 30(12), pp. 8913–8925. DOI: 10.1007/s11665-021-06115-2.
[39] Ahmadi-Moghadam, B., Taheri, F. (2014). Fracture and toughening mechanisms of GNP-based nanocomposites in modes I and II fracture, Engineering Fracture Mechanics, 131, pp. 329–339. DOI: 10.1016/j.engfracmech.2014.08.008.
[40] Kang, W.S., Rhee, K.Y., Park, S.J. (2016). Thermal, impact and toughness behaviors of expanded graphite/graphite oxide-filled epoxy composites, Composites Part B: Engineering, 94, pp. 238–244. DOI: 10.1016/j.compositesb.2016.03.052.
[41] Khan, S.U., Pothnis, J.R., Kim, J.K. (2013). Effects of carbon nanotube alignment on electrical and mechanical properties of epoxy nanocomposites, Composites Part A: Applied Science and Manufacturing, 49, pp. 26–34. DOI: 10.1016/j.compositesa.2013.01.015.
[42] Bisht, A., Dasgupta, K., Lahiri, D. (2018). Effect of graphene and CNT reinforcement on mechanical and thermomechanical behavior of epoxy-A comparative study, Journal of Applied Polymer Science, 135(14), p. 46101. DOI: 10.1002/app.46101.
[43] Rasul, M.G., Kiziltas, A., Arfaei, B., Shahbazian-Yassar, R. (2021). 2D boron nitride nanosheets for polymer composite materials, Npj 2D Materials and Applications, 5(1), p. 56. DOI: 10.1038/s41699-021-00231-2.

[44] Frigione, M., Lettieri, M. (2020). Recent advances and trends of nanofilled/nanostructured epoxies, Materials, 13(15), p. 3415. DOI: 10.3390/ma13153415.
[45] Buragohain, M.K. (2017). Composite structures: Design, mechanics, analysis, manufacturing and testing, Boca Raton, CRC Press, DOI: 10.1201/9781315268057.
[46] Joy, J., George, E., Haritha, P., Thomas, S., Anas, S. (2020). An overview of boron nitride based polymer nanocomposites, Journal of Polymer Science, 58(22), pp. 3115–3141. DOI: 10.1002/pol.20200507.
[47] Wang, F., Bai, C., Chen, L., Yu, Y. (2021). Boron nitride nanocomposites for microwave absorption: A review, Materials Today Nano, 13, p. 100108. DOI: 10.1016/j.mtnano.2020.100108.
[48] Rouhi, S. (2016). Molecular dynamics simulation of the adsorption of polymer chains on CNTs, BNNTs and GaNNTs, Fibers and Polymers, 17(3), pp. 333–342. DOI: 10.1007/s12221-016-5676-8.
[49] Patki, A.M., Goyal, R.K. (2021). Investigation of non-isothermal crystallization, dynamic mechanical and dielectric properties of poly(ether-ketone) matrix composites, Polymer-Plastics Technology and Materials, 60(1), pp. 70–83. DOI: 10.1080/25740881.2020.1786583.
[50] Kavimani, V., Gopal, P.M., Stalin, B., Karthick, A., Arivukkarasan, S., Bharani, M. (2021). Effect of graphene oxide-boron nitride-based dual fillers on mechanical behavior of epoxy/glass fiber composites, Journal of Nanomaterials, 2021, pp. 1–10. DOI: 10.1155/2021/5047641.
[51] Patki, A.M., Goyal, R.K. (2019). High performance polyetherketone-hexagonal boron nitride nanocomposites for electronic applications, Journal of Materials Science: Materials in Electronics, 30(4), pp. 3899–3908. DOI: 10.1007/s10854-019-00675-9.
[52] Liu, L., Xiao, L., Li, M., Zhang, X., Chang, Y., Shang, L., Ao, Y. (2016). Effect of hexagonal boron nitride on high-performance polyether ether ketone composites, Colloid and Polymer Science, 294(1), pp. 127–133. DOI: 10.1007/s00396-015-3733-2.
[53] Chen, B., Ni, B.J., Fu, M.X., Zhong, H., Jiang, W.F., Liu, S.Y., Zhang, H.X., Yoon, K.B. (2019). Effect of molybdenum disulfide exfoliation conditions on the mechanical properties of epoxy nanocomposites, Chinese Journal of Polymer Science, 37(7), pp. 687–692. DOI: 10.1007/s10118-019-2239-7.
[54] ASTM International. (2014). ASTM D5045, Standard test methods for plane-strain fracture toughness and strain energy release rate of plastic materials, West Conshohocken, PA, DOI: 10.1520/D5045-14.
[55] ASTM International. (2017). ASTM E1820, Standard test method for measurement of fracture toughness, West Conshohocken, PA, DOI: 10.1520/E1820-17.
[56] Bakker, A. (1990). Compatible compliance and stress intensity expressions for the standard three-point bend specimen, Fatigue & Fracture of Engineering Materials and Structures, 13(2), pp. 145–154. DOI: 10.1111/j.1460-2695.1990.tb00586.x.
[57] Fett, T. (1991). Mixed-mode stress intensity factors for three-point bending bars, International Journal of Fracture, 48(4), pp. R67–R74. DOI: 10.1007/BF00012920.
[58] Fett, T., Gerteisen, G., Hahnenberger, S., Martin, G., Munz, D. (1995). Fracture tests for ceramics under mode-I, mode-II and mixed-mode loading, Journal of the European Ceramic Society, 15(4), pp. 307–312. DOI: 10.1016/0955-2219(95)90353-K.
[59] Wang, D., Zhou, K., Yang, W., Xing, W., Hu, Y., Gong, X. (2013). Surface modification of graphene with layered molybdenum disulfide and their synergistic reinforcement on reducing fire hazards of epoxy resins, Industrial & Engineering Chemistry Research, 52(50), pp. 17882–17890. DOI: 10.1021/ie402441g.
[60] González, M.G., Cabanelas, J.C., Baselga, J. (2012). Applications of FTIR on epoxy resins - identification, monitoring the curing process, phase separation and water uptake., In: Theophile, T. ed., Infrared Spectroscopy - Materials Science, Engineering and Technology, United Kingdom, InTech.
[61] Pavia, D.L., Lampman, G.M., Kriz, G.S., Vyvyan, J.R. (2015). Introduction to spectroscopy, 5th ed., Washington DC, Cengage Learning.
[62] Aradi, E., Naidoo, S.R., Billing, D.G., Wamwangi, D., Motochi, I., Derry, T.E. (2014). Ion beam modification of the structure and properties of hexagonal boron nitride: An infrared and X-ray diffraction study, Nuclear Instruments and Methods in Physics Research Section B: Beam Interactions with Materials and Atoms, 331, pp. 140–143. DOI: 10.1016/j.nimb.2014.01.031.
[63] Tsuji, Y., Kitamura, Y., Someya, M., Takano, T., Yaginuma, M., Nakanishi, K., Yoshizawa, K. (2019). Adhesion of epoxy resin with hexagonal boron nitride and graphite, ACS Omega, 4(3), pp. 4491–4504. DOI: 10.1021/acsomega.9b00129.

[64] Chen, B., Zhang, M., Li, X., Dong, Z., Jia, Y., Li, C. (2020). Tribological properties of epoxy-based self-lubricating composite coating enhanced by 2D/2D h-BN/MoS_2 hybrid, Progress in Organic Coatings, 147, p. 105767. DOI: 10.1016/j.porgcoat.2020.105767.
[65] Wang, Y., Zhao, D. (1995). Characterization of interlaminar fracture behaviour of woven fabric reinforced polymeric composites, Composites, 26(2), pp. 115–124. DOI: 10.1016/0010-4361(95)90411-R.
[66] Rao, Y.S., Mohan, N.S., Shetty, N., Shivamurthy, B. (2021). Effects of solid lubricant fillers on the flexural and shear strength response of carbon fabric-epoxy composites, Polymer Testing, 96, p. 107085. DOI: 10.1016/j.polymertesting.2021.107085.
[67] Johnsen, B.B., Kinloch, A.J., Mohammed, R.D., Taylor, A.C., Sprenger, S. (2007). Toughening mechanisms of nanoparticle-modified epoxy polymers, Polymer (Guildf), 48(2), pp. 530–541. DOI: 10.1016/j.polymer.2006.11.038.
[68] Saravanakumar, K., Arumugam, V., Souhith, R., Santulli, C. (2020). Influence of milled glass fiber fillers on mode I & mode II interlaminar fracture toughness of epoxy resin for fabrication of glass/epoxy composites, Fibers, 8(6), p. 36. DOI: 10.3390/fib8060036.
[69] Argüelles, A., Viña, J., Canteli, A.F., Bonhomme, J. (2009). Fatigue delamination, initiation, and growth, under mode I and II of fracture in a carbon-fiber epoxy composite, Polymer Composites, 31(4), pp. 700–706. DOI: 10.1002/pc.20855.
[70] Agarwal, B.D., Broutman, L.J., Chandrashekhara, K. (2015). Analysis and performance of fiber composites, 3rd ed., Hoboken, USA, John Wiley & Sons, Inc.
[71] Rakshit, D., Chakraborty, S. (2015). Determination of fracture parameters of FRP composites: A combined experimental and numerical investigation, Journal of Composite Materials, 49(2), pp. 231–241. DOI: 10.1177/0021998313516142.
[72] Rodríguez-García, V., Herráez, M., Martínez, V., Guzman de Villoria, R. (2022). Interlaminar and translaminar fracture toughness of automated manufactured bio-inspired CFRP laminates, Composites Science and Technology, 219, p. 109236. DOI: 10.1016/j.compscitech.2021.109236.
[73] Yu, L., Yang, S., Liu, W., Xue, Q. (2000). Investigation of the friction and wear behaviors of polyphenylene sulfide filled with solid lubricants, Polymer Engineering and Science, 40(8), pp. 1825–1832. DOI: 10.1002/pen.11314.
[74] Srivastava, S.K., Sahoo, A.K., Bindumadhavan, K., Manu, S.K., Nayak, B.B., Biswas, K., Saxena, A.K., Singh, R. (2010). Reinforcement of ball shaped MoS_2 nanoparticles in epoxy resin, Journal of Nanoscience and Nanotechnology, 10(12), pp. 8171–8179. DOI: 10.1166/jnn.2010.3544.
[75] Ahamad, T., Alshehri, S.M. (2013). Thermal degradation and evolved gas analysis of epoxy (DGEBA)/novolac resin blends (ENB) during pyrolysis and combustion, Journal of Thermal Analysis and Calorimetry, 111(1), pp. 445–451. DOI: 10.1007/s10973-012-2431-2.
[76] Grund, D., Orlishausen, M., Taha, I. (2019). Determination of fiber volume fraction of carbon fiber-reinforced polymer using thermogravimetric methods, Polymer Testing, 75, pp. 358–366. DOI: 10.1016/j.polymertesting.2019.02.031.
[77] Ramdani, N. (2019). Polymer and ceramic composite materials, 1st ed., Boca Raton, CRC Press, DOI: 10.1201/b22371.
[78] Kumar, R., Mishra, A., Sahoo, S., Panda, B.P., Mohanty, S., Nayak, S.K. (2019). Epoxy-based composite adhesives: Effect of hybrid fillers on thermal conductivity, rheology, and lap shear strength, Polymers for Advanced Technologies, 30(6), pp. 1365–1374. DOI: 10.1002/pat.4569.
[79] Ren, J., Li, Q., Yan, L., Jia, L., Huang, X., Zhao, L., Ran, Q., Fu, M. (2020). Enhanced thermal conductivity of epoxy composites by introducing graphene@boron nitride nanosheets hybrid nanoparticles, Materials & Design, 191, p. 108663. DOI: 10.1016/j.matdes.2020.108663.
[80] Zheng, X., Kim, S., Park, C.W. (2019). Enhancement of thermal conductivity of carbon fiber-reinforced polymer composite with copper and boron nitride particles, Composites Part A: Applied Science and Manufacturing, 121, pp. 449–456. DOI: 10.1016/j.compositesa.2019.03.030.
[81] Coats, A.W., Redfern, J.P. (1964). Kinetic parameters from thermogravimetric data, Nature, 201(4914), pp. 68–69. DOI: 10.1038/201068a0.